



Area tensors for modeling microstructure during laminar liquid-liquid mixing

E.D. Wetzel, C.L. Tucker III*

Department of Mechanical and Industrial Engineering, University of Illinois at Urbana-Champaign, Urbana, IL 61801, U.S.A.

Received 17 October 1997; received in revised form 20 May 1998

Abstract

Fluid-fluid mixtures often possess a fine structure, or morphology, whose length scale is much smaller than the length scale over which the flow field and morphology vary. We define a microstructural variable called the *area tensor*, which describes the local morphology of such mixtures through volume-averaged size, shape, and orientation characteristics. The area tensor is equivalent to the interface tensor of the rheological model, and is closely related to the general microstructural tensors. The evolution equation for the area tensor during laminar mixing is derived for the case of equal component viscosities and negligible surface tension. Solution of this evolution equation requires a closure approximation for estimating higher-order microstructural statistics. A closure approximation is generated based on exact area tensor relations for ellipsoidal shapes, and is shown to provide highly accurate evolutions of the area tensor. Area tensor histories are calculated in homogeneous elongational and shearing flows, as well as in temporally and spatially varying flows. The results are shown to be consistent with well-known mixing principles. © 1999 Elsevier Science Ltd. All rights reserved.

Keywords: Mixing; Area tensor; Closure approximation; Microstructured fluids; Polymer blend; Interface tensor

1. Introduction

Laminar mixing of immiscible fluids occurs frequently in both natural and industrial processes. Often the mixture assumes a structure which is very fine-scaled, such that the characteristic size of the mixture structure is much less than the length scale of the overall mixing domain. In such a case the mixture is said to possess a morphology. Examples of such

* Corresponding author.

mixing processes include blending of polymers, and tectonic shearing of inclusions in the Earth's lower crust.

Due to the fineness of the mixture structure, tracking the exact configuration of each phase throughout the entire mixture is impractical. Instead, we assume that each material point in the mixture is associated with a finite volume whose characteristic size is much larger than the characteristic length scale of the mixture structure, but is still smaller than the size of the overall mixing domain. The mixture morphology at each material point is represented in terms of some measure that summarizes the basic features of the microstructure within this local volume. Since the volume is much smaller than the overall mixing domain, this local measure can be treated as a field variable, and is capable of reflecting spatial variations in morphology over the mixing domain. For mixing analyses, we further assume that the characteristic size of the averaging volume is small enough such that the velocity and deformation fields are approximately linear within it. The evolution of the morphology can then be modeled by predicting the change in the local morphological measure due to this velocity or deformation gradient. We will call such an approach, which treats some local characteristic morphological measure as a field variable, a *micromixing* analysis.

The micromixing approach has been used extensively for modeling *passive mixing*, where interfacial energy is negligible and the two phases have identical viscosities. In passive mixing the global velocity field can be found independently of the microstructure and then used to evolve the mixture structure. Spencer and Wiley (1951) presented one of the earliest micromixing analyses. They noted that many passive mixtures assume striated structures which can be modeled by studying the evolution of passive material surfaces. They also established that a fundamental process in mixing is the growth of interfacial area, and that the orientation of this area relative to the flow field significantly influences mixing efficiency. Mohr et al (1957) defined specific area as a local measure of mixing, and found that it is the inverse of the striation thickness for lamellar structures. They also showed that interfacial area grows linearly in shearing flows. Erwin (1978) demonstrated that much greater mixing efficiency is possible in extensional flows, where interfacial area grows exponentially with deformation. Finally, Ottino et al. (1981) and Chella and Ottino (1985) derived general formulas for the deformation of lamellae in arbitrary deformation fields, essentially “solving” the problem of passive mixing for lamellar structures.

The purpose of morphology modeling is to enable the prediction and control of mixture properties. These properties include mixture rheology during processing, as well as mixture appearance, permeability, and mechanical properties after processing. To predict many mixture properties, the local size, orientation, and shape of the microstructure must be known. The existing treatments of passive micromixing provide size and orientation information, but only for lamellar structures. Real mixture morphologies are often not lamellar, forming droplets, cylinders, and other shapes, either due to non-lamellar initial conditions or due to the presence of interfacial tension. While passive mixing by definition excludes interfacial tension effects, the development of a passive mixing model which can handle non-lamellar geometries is a necessary precursor to the modeling of non-passive mixing. Therefore, there is a need for a more general passive micromixing model, one which is capable of predicting size, orientation, and shape information.

In this paper we present a new approach for modeling passive micromixing. We introduce a variable, called the area tensor, that represents the size, shape, and orientation of the local morphology. We also provide an accurate and efficient means to predict the evolution of this variable during passive mixing, and show its applicability to predicting morphological gradients in non-homogenous flows. Finally, we demonstrate that the area tensor approach permits the incorporation of other physical effects, such as interfacial tension, and therefore has great promise for modeling non-passive micromixing as well.

2. Area tensors

2.1. Definition of area tensors

Consider the mixture shown in Fig. 1, where the scale of the microstructure is sufficiently fine that exact modeling of the phases throughout the entire mixture is not feasible. We instead associate some volume V with each material point P within the mixture. In accordance with the micromixing approach, V is much smaller than the overall mixing domain, but larger than the characteristic size of the microstructure. The morphology ‘at P ’ is then defined as the morphology within V .

The morphology of a binary liquid mixture can be modeled by tracking the interface between the two phases. One possible approach is to discretize the interface within V into an array of differential elements, each with some area dS and unit normal vector $\hat{\mathbf{n}}$. In order to model the evolution of the morphology during flow, the rotation, translation, and deformation of each of these differential areas could be tracked. However, this strategy is computationally expensive and, when modeled over the entire mixture, provides an overwhelming amount of information.

A more efficient and useful means of modeling microstructural evolution is to track selected statistics of the interfaces associated with each material point. One such statistical representation is the *area tensor*, which we define as

$$\mathbf{A} \equiv \frac{1}{V} \int_{\Gamma} \hat{\mathbf{n}} \hat{\mathbf{n}} dS \quad (1)$$

where the integral is taken over the entire interfacial surface Γ within the averaging volume V .

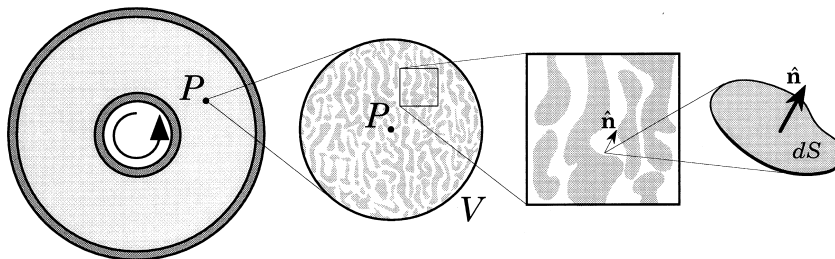
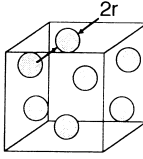
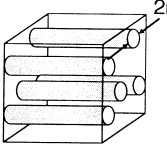
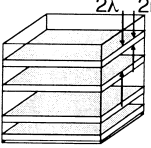


Fig. 1. Length scales in a fine-scaled mixture.

Table 1
Characteristics of special morphologies

Geometry	\mathbf{A}	L_c
Spherical 	$S_V \begin{bmatrix} \frac{1}{3} & 0 & 0 \\ 0 & \frac{1}{3} & 0 \\ 0 & 0 & \frac{1}{3} \end{bmatrix}$	$r/3$
Cylindrical 	$S_V \begin{bmatrix} \frac{1}{2} & 0 & 0 \\ 0 & \frac{1}{2} & 0 \\ 0 & 0 & 0 \end{bmatrix}$	$r/2$
Lamellar 	$S_V \begin{bmatrix} 1 & 0 & 0 \\ 0 & 0 & 0 \\ 0 & 0 & 0 \end{bmatrix}$	$r = \phi\lambda$

(Bold lowercase letters represent vectors and bold uppercase letters represent second-order tensors. Vectors with unit magnitude and second-order tensors with unit trace are indicated by a hat, $\hat{\cdot}$). This second-order area tensor is a local volume average of the dyadic product of each normal vector with itself, and has units of surface area per unit volume.

It is possible to define area tensors of any order, such as the fourth-order area tensor

$$\mathcal{A} \equiv \frac{1}{V} \int_V \hat{\mathbf{n}} \hat{\mathbf{n}} \hat{\mathbf{n}} \hat{\mathbf{n}} dS. \quad (2)$$

(Fourth-order tensors are represented with the calligraphic font). Only the even-order area tensors are useful because the components of odd-order area tensors are zero-valued when the interfaces within V are closed surfaces. Throughout this paper the term “area tensor” refers to the second-order area tensor unless otherwise stated.

2.2. Properties of area tensors

2.2.1. General characteristics

The area tensor contains considerable information about the local morphology of the mixture, including the size, shape, and orientation of the microstructure.

The trace of the area tensor equals the total interfacial area per unit volume, also known as the specific area S_V

$$\text{tr}(\mathbf{A}) = S/V \equiv S_V. \quad (3)$$

In classical mixing theory the specific area has special significance. Mohr et al. (1957) first used

the striation thickness λ (see Table 1), defined as one-half the spacing between layer midplanes in a lamellar structure, as a measure of mixing. Striation thickness is related to the specific area of a lamellar mixture by

$$\lambda = \frac{1}{S_V}. \quad (4)$$

Specific area is a zeroth-order area tensor, containing only magnitude information. The second-order area tensor extends this classical mixing measure to incorporate shape and orientation effects.

It is convenient to define a normalized area tensor $\hat{\mathbf{A}}$ as

$$\hat{\mathbf{A}} \equiv \mathbf{A}/S_V. \quad (5)$$

Because the area tensor is real and symmetric, its principal values are real and its principal directions are orthogonal. When rotated to its principal axis system, the normalized area tensor is written as

$$\bar{\hat{\mathbf{A}}} = \begin{bmatrix} \hat{A}_{(1)} & 0 & 0 \\ 0 & \hat{A}_{(2)} & 0 \\ 0 & 0 & \hat{A}_{(3)} \end{bmatrix} \quad (6)$$

where the overbar denotes a rotated tensor. For uniqueness, we choose a rotation such that the eigenvalues are numbered in order of decreasing magnitude,

$$\hat{A}_{(1)} \geq \hat{A}_{(2)} \geq \hat{A}_{(3)}. \quad (7)$$

The principal directions of the tensor indicate the most and least likely orientations for interfacial area, and the eigenvalues of $\hat{\mathbf{A}}$ reflect the relative amounts of interfacial area oriented in each principal direction.

2.2.2. Example area tensors

When the mixture has one discrete and one continuous phase, the area tensor provides information about the shape and size of the discrete-phase domains. Table 1 shows the area tensors for three example mixture morphologies. The area tensor is triaxial (isotropic) for spherical domains, biaxial (transversely isotropic) for cylindrical domains, and uniaxial for lamellar structures.

In the most general case, the volume fraction of discrete phase ϕ could be modeled as a spatially varying quantity that is advected with the fluid. For this study we will assume that the mixture components are well distributed on large length scales, so that ϕ is uniform throughout the mixture. Such a situation arises in many polymer processing operations, where the components are either well mixed as solid pellets before melting, or the pellets themselves are pre-blended. We can then define a local characteristic length scale L_c for the discrete phase as the ratio of the total volume V_d of the discrete phase within V to the total interfacial area S_d within V

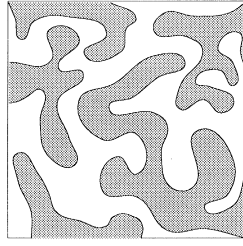


Fig. 2. A co-continuous microstructure.

$$L_c \equiv V_d/S_d = \phi/S_V. \quad (8)$$

Table 1 gives the characteristic length scales for the three example morphologies. The characteristic radius of the lamellar structure is related to the striation thickness by $r = \phi \lambda$.

It is also possible to interpret the area tensor in terms of the number density of discrete-phase domains. For a monodisperse mixture, the number of domains per unit volume N_V is given by

$$N_V = \phi/V_c = S_V/S_c \quad (9)$$

where V_c and S_c are the volume and surface area of a single domain with characteristic size L_c .

When there is no discrete phase, the area tensor is still well defined. Some mixtures form co-continuous structures, like that shown in Fig. 2. A three-dimensionally random co-continuous structure will have the same area tensor as a spherical structure, since the interface is distributed isotropically in both morphologies. While the area tensor can represent either structure, one cannot distinguish between the two structures solely on the basis of their area tensors.

2.3. Ellipsoidal interpretation of area tensors

In passive micromixing the local deformation field varies linearly with position, so that an initially spherical discrete domain will deform into an ellipsoid for any state of strain. The area tensor uniquely defines the size, shape, and orientation of such an ellipsoid. This characteristic ellipsoid provides a convenient way to interpret the area tensor.

Consider a general ellipsoid with semiaxis lengths r_1 , r_2 , and r_3 ,

$$\frac{z_1^2}{r_1^2} + \frac{z_2^2}{r_2^2} + \frac{z_3^2}{r_3^2} = 1 \quad (10)$$

where z_1 , z_2 , and z_3 are coordinates along the principal axes of the ellipsoid. For convenience, we number the axes so that $r_3 \geq r_2 \geq r_1$. It is possible to solve exactly for the principal values of the normalized area tensor in terms of the semi-axis ratios

$$C = \frac{r_1}{r_3}, \quad D = \frac{r_1}{r_2} \quad (11)$$

by integrating (1) over the surface of the ellipsoid. The axes of the ellipsoid, z_1 , z_2 , and z_3 , are

the principal directions of the tensor, so we need only consider the diagonal components of $\hat{\mathbf{A}}$. The resulting exact relationships are (Appendix A)

$$\hat{A}_{(1)} = \frac{1}{1 - D^2} \frac{E(\theta, k) - D^2 F(\theta, k)}{(1 - C^2)E(\theta, k) + C^2 F(\theta, k) + CD\sqrt{1 - C^2}}, \quad (12)$$

$$\hat{A}_{(2)} = \frac{D^2}{D^2 - C^2} \frac{\frac{D^2 - C^2}{1 - D^2} F(\theta, k) - D^2 \frac{1 - C^2}{1 - D^2} E(\theta, k) CD\sqrt{1 - C^2}}{(1 - C^2)E(\theta, k) + C^2 F(\theta, k) + CD\sqrt{1 - C^2}}, \quad (13)$$

$$\hat{A}_{(3)} = \frac{C^2}{D^2 - C^2} \frac{C^2 E(\theta, k) + (D^2 - C^2)F(\theta, k) - CD\sqrt{1 - C^2}}{(1 - C^2)E(\theta, k) + C^2 F(\theta, k) + CD\sqrt{1 - C^2}} \quad (14)$$

where

$$k = \sqrt{\frac{1 - D^2}{1 - C^2}}, \quad (15)$$

$$\theta = \cos^{-1}(C) \quad (16)$$

and $F(\theta, k)$ and $E(\theta, k)$ are elliptic integrals of the first and second kind, respectively, as defined in Gradshteyn and Ryzhik (1994).

These exact relationships cannot be inverted analytically, and therefore cannot be used directly to infer shape information from the area tensor components. However, we have found that the semi-axis ratios are well approximated by

$$C \cong \left(\frac{\hat{A}_{(3)}}{\hat{A}_{(1)}} \right)^\alpha, \quad D \cong \left(\frac{\hat{A}_{(2)}}{\hat{A}_{(1)}} \right)^\alpha \quad (17)$$

with $\alpha = 0.5977$. The semi-axis ratio values from this approximation are exact for the limiting cases of uniaxial, biaxial, and isotropic tensors, and they fall within 0.04 of the exact values for all other ellipsoidal shapes.

The size scaling for a given area tensor is provided by its trace, or the specific area. For a general ellipsoid, the exact characteristic length, as defined in (8), is

$$L_c = \frac{2}{3} r_1 \left[CD + \sqrt{1 - C^2} E(\theta, k) + \frac{C^2}{\sqrt{1 - C^2}} F(\theta, k) \right]^{-1}. \quad (18)$$

A more tractable formulation for characteristic radius can be derived by using the approximations for ellipsoidal surface area recommended by Lehmer (1950).

$$L_c \cong r_1 \left[\frac{2}{5} (C + D + 1) + \frac{3}{5} \sqrt{3(C^2 + D^2 + 1)} \right]^{-1}. \quad (19)$$

This approximation is within 5% of the exact value of L_c for all possible ellipsoidal shapes.

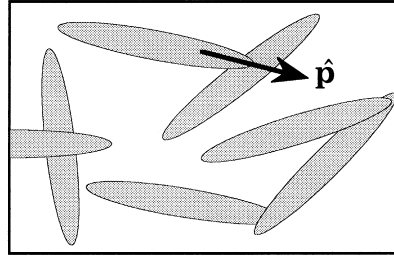


Fig. 3. Collection of axisymmetric particles, each described by a unit vector $\hat{\mathbf{p}}$.

Using (8, 11, 17, 19), one can interpret any area tensor and discrete-phase volume fraction ϕ in terms of a representative ellipsoidal size and shape. The principal axes of \mathbf{A} are the principal axes of the ellipsoid.

2.4. Relationship to other microstructural variables

The local microstructure for suspensions of rigid, axisymmetric particles is frequently described by a microstructural tensor \mathbf{M} (Hinch and Leal, 1976), defined as

$$\mathbf{M} = \langle \hat{\mathbf{p}}\hat{\mathbf{p}} \rangle. \quad (20)$$

Here $\hat{\mathbf{p}}$ is a unit vector parallel to the symmetry axis of each particle (Fig. 3). The angle brackets denote an average over all the particles in the local averaging volume.

Similarly, the area tensor describes the local orientation distribution of the differential areas which compose the interfacial surface. Each differential area is analogous to a thin disk with area dS and an orientation axis defined by the normal $\hat{\mathbf{n}}$. Unlike the identical rigid particles which compose the tensor \mathbf{M} , each differential area is weighted differently in the average according to its magnitude dS . Since the differential areas are deformed by the flow, the trace of the area tensor can change, whereas the trace of the tensor \mathbf{M} is fixed.

Doi (1987) and others (Rosenkilde, 1967; Batchelor, 1970) have shown that in a blend of immiscible fluids the contribution of the interfacial tension σ to the extra stress is $-\sigma q_{ij}$, where q_{ij} is the *interface tensor*, defined as

$$q_{ij} = \frac{1}{V} \int_{\Gamma} \left(n_i n_j - \frac{1}{3} \delta_{ij} \right) dS \quad (21)$$

and δ_{ij} is the Kronecker delta. (In order to be consistent with the literature, here we relax the convention that tensors must be capital letters.) In Doi and Ohta's rheological model for a blend of two immiscible fluids with identical viscosity, the microstructure is described by the interface tensor and by the total interfacial area per unit volume, Q in their notation. Their model has demonstrated considerable potential for explaining the complex rheological behavior of blends of immiscible fluids (Takahashi et al., 1994; Guenther and Baird, 1996; Vinckier et al., 1996). Extensions to the theory have been proposed by Lee and Park (1994), retaining the same microstructural variables.

The interface tensor is directly related to the area tensor, since

$$Q = S_V = A_{ii}, \quad (22)$$

$$q_{ij} = A_{ij} - \frac{1}{3} S_V \delta_{ij}. \quad (23)$$

The interface tensor is the deviatoric part of the area tensor, and Q is the hydrostatic part. Thus, the Doi–Ohta model and its variations can be re-cast with the area tensor as the microstructural variable.

The interface tensor is convenient for rheological models because of its direct relationship to stress. For morphological modeling, the area tensor has the advantages that it contains both q_{ij} and Q in one quantity, and it is consistent with the microstructural tensors of Hinch and Leal (1976). The latter feature will prove useful for the formation of a closure approximation in Section 4, and should also facilitate development of area tensor–based property predictions.

3. Evolution equation

3.1. Passive mixing

Passive mixing involves two fluids with identical rheology and negligible interfacial tension. Under these conditions the macroscopic and microscopic velocity fields are identical, and interfaces rotate and stretch as material surfaces in response to the macroscopic velocity field. For a micromixing analysis, we assume that the size of the averaging volume V is small enough that the velocity field within V is approximately linear, and all interfaces within V deform according to the velocity gradient tensor at the associated material point P . We can then formulate an evolution equation for the area tensor at P based only on the velocity gradient tensor at P . A similar argument holds for the formation of a finite strain equation for the area tensor based on the local deformation gradient tensor.

3.1.1. Differential formulation

Using the definition of the area tensor, (1), and the chain rule, the rate of change of the area tensor is

$$\dot{\mathbf{A}} = \frac{1}{V} \int_{\Gamma} \dot{\mathbf{n}} \mathbf{n} dS + \frac{1}{V} \int_{\Gamma} \mathbf{n} \dot{\mathbf{n}} dS + \frac{1}{V} \int_{\Gamma} \mathbf{n} \mathbf{n} \dot{S} \quad (24)$$

where the dot signifies a material derivative. For passive mixing Chella and Ottino (1985) showed that the normal vector of a differential area rotates as

$$\dot{\hat{n}}_i = -L_{ji} \hat{n}_j + (L_{jk} \hat{n}_j \hat{n}_k) \hat{n}_i \quad (25)$$

and, for an incompressible fluid, the magnitude of the differential area changes as

$$d\dot{S} = -(L_{jk} \hat{n}_j \hat{n}_k) dS. \quad (26)$$

(When indicial notation is used, repeated indices imply summation.) Here \mathbf{L} is the velocity gradient tensor, $L_{ij} = \partial v_i / \partial x_j$. Under the passive micromixing assumption, V is sufficiently small that all differential areas within V experience the same velocity gradient. We can then substitute (25, 26) into (24) which, after simplification, yields the desired evolution equation for the area tensor

$$\dot{A}_{ij} = -L_{ki}A_{kj} - A_{ik}L_{kj} + L_{kl}A_{klj} \quad (27)$$

where \mathcal{A} is the fourth-order area tensor defined in (2). Note that this equation is exact for passive micromixing in any flow field, regardless of whether the mixture contains discrete droplets, co-continuous phases, or has any other morphology.

Replacing the velocity gradient by the rate of deformation tensor $E_{ij} = (L_{ij} + L_{ji})/2$ and the vorticity tensor $\Omega_{ij} = (L_{ij} - L_{ji})/2$ in (27) and rearranging yields

$$\dot{A}_{ij} - \Omega_{ik}A_{kj} + A_{ik}\Omega_{kj} = -(E_{ik}A_{kj} + A_{ik}E_{kj} - E_{kl}A_{klj}). \quad (28)$$

The left-hand side of this equation is a co-rotating Jaumann derivative. The fact that the co-rotating derivative is a function only of the microstructure and \mathbf{E} guarantees that our evolution equation satisfies the principle of coordinate frame indifference. Alternately, if (28) is rearranged to isolate the term containing \mathcal{A} on the right-hand side, then the left-hand side is found to be the lower convected derivative of \mathbf{A} .

Taking the trace of (28) yields a simple relation for the rate of area growth, an important measure of mixing efficiency,

$$\dot{A}_{ii} = \dot{S}_V = -E_{jk}A_{jk}. \quad (29)$$

For lamellar structures this equation reduces to Chella and Ottino's expression for area growth, (26). But unlike Chella and Ottino's result, (29) applies to any geometric arrangement of interfaces. Therefore, the area tensor is the fundamental quantity governing the rate of area growth during passive mixing for all microstructures.

The exact evolution equation for the second-order tensor, (27), requires the fourth-order tensor, which we do not track explicitly. Similarly, evolving the fourth-order tensor exactly would require higher-order statistical information. The dependence of the second-order area tensor evolution equation on higher-order statistics presents a closure problem, a common feature of tensorial microstructural models. To evolve the second-order tensor on the basis of second-order statistics alone, we can approximate the fourth-order tensor in terms of the second-order tensor with a *closure approximation*. The derivation of an accurate closure approximation for area tensor evolution during passive mixing is the focus of Section 4.

3.1.2. Finite strain formulation

In this section we explore the possibility of a finite strain area tensor evolution equation. The assumption of passive interfaces guarantees the existence of a well-defined mapping between the initial position x^0 of a material point and its position x at any time during the flow history. In the vicinity of any point, this mapping is described by the deformation gradient tensor \mathbf{F} , defined as $\mathbf{F} = \partial \mathbf{x} / \partial \mathbf{x}^0$.

If the deformation gradient tensor acts on a differential area with initial magnitude dS^0 and normal vector $\hat{\mathbf{n}}^0$, the differential area deforms to a new magnitude dS . The area stretch, $\eta \equiv dS/dS^0$, is given by

$$\eta = \det \mathbf{F} \sqrt{(\mathbf{F}^T \mathbf{F})^{-1} \cdot \hat{\mathbf{n}}^0 \hat{\mathbf{n}}^0}. \quad (30)$$

The deformation also causes the initial unit normal vector $\hat{\mathbf{n}}^0$ to rotate to a new direction $\hat{\mathbf{n}}$ according to

$$\hat{\mathbf{n}} = \frac{1}{\eta} (\det \mathbf{F}) (\mathbf{F}^{-1})^T \hat{\mathbf{n}}^0 \quad (31)$$

(Chella and Ottino, 1985). Under the micromixing assumption, V is sufficiently small that all differential areas within V experience the same deformation gradient. We can then substitute (30, 31) into the definition of the area tensor, (1), and simplify to yield

$$\mathbf{A} = (\det \mathbf{F}) (\mathbf{F}^{-1})^T \left(\frac{1}{V} \int_{\Gamma} \frac{\hat{\mathbf{n}}^0 \hat{\mathbf{n}}^0}{\sqrt{(\mathbf{F}^T \mathbf{F})^{-1} \cdot \hat{\mathbf{n}}^0 \hat{\mathbf{n}}^0}} dS^0 \right) \mathbf{F}^{-1}. \quad (32)$$

For evolving area tensors, we seek a finite strain mapping of the initial area tensor \mathbf{A}^0 , defined as

$$\mathbf{A}^0 = \frac{1}{V} \int_{\Gamma} \hat{\mathbf{n}}^0 \hat{\mathbf{n}}^0 dS^0 \quad (33)$$

into the area tensor \mathbf{A} for any deformation state \mathbf{F} . However, (32) shows that such a formulation is not possible in terms of \mathbf{F} and \mathbf{A}^0 alone. This limitation is analogous to the closure problem encountered in the differential formulation. However, unlike the differential formulation, we know of no systematic method for approximating the finite strain evolution equation in terms of the second-order area tensor alone. Furthermore, only the differential formulation provides a means of incorporating rate effects associated with dispersion phenomena. Therefore, only the differential formulation for area tensor evolution will be pursued further.

3.2. Incorporation of additional process physics

An attractive feature of the rate formulation is that additional physical phenomena can readily be incorporated into the model. For two fluids with identical viscosity the effects of interfacial tension σ can be represented by adding a term \mathbf{P} to the evolution equation:

$$\dot{A}_{ij} = -L_{ki} A_{kj} - A_{ik} L_{kj} + L_{kl} A_{klj} + P_{ij}. \quad (34)$$

The Doi and Ohta (1991) rheological model contains a relaxation term of this type, through which interfacial tension drives the microstructure to an isotropic state while decreasing the specific surface area. That theory can be re-cast into the form of (34) by choosing

$$P_{ij} = -\lambda^* \frac{\sigma}{\mu} S_V^2 \left[\left(\hat{A}_{ij} - \frac{1}{3} \delta_{ij} \right) - \frac{1}{3} \mu^* \delta_{ij} \right]. \quad (35)$$

Here μ is the fluid viscosity, and λ^* and μ^* are constants related to the volume fraction of the dispersed phase.

Doi and Ohta's original model has the undesirable feature that, for long times without flow, $S_V \rightarrow 0$. Lee and Park (1994) proposed modifications to the Doi-Ohta model that are intended to correct the limiting behavior of the relaxation term, to account for unequal component viscosities in stress calculations, and to model droplet break-up and coalescence. Their model can similarly be cast into the form of (34) by choosing an appropriate expression for \mathbf{P} (Wetzel and Tucker, 1997a).

The differential form of the area tensor evolution equation provides a general framework within which many models for additional process physics can be included. For the remainder of this study we restrict our attention to mixtures with passive interfaces, so that \mathbf{P} is neglected.

3.3. Relationship to particle evolution equations

When a collection of rigid, axisymmetric particles is described by the microstructural tensor of (20), the evolution equation (in the absence of Brownian motion) is (Hinch and Leal, 1976)

$$\dot{M}_{ij} - \Omega_{ik} M_{kj} + M_{ik} \Omega_{kj} = \epsilon (E_{ik} M_{kj} + M_{ik} E_{kj} - 2E_{kl} M_{klj}). \quad (36)$$

Here ϵ is a constant that accounts for the particle shape, taking on the special values $\epsilon = 1$ for slender fibers, and $\epsilon = -1$ for thin disks.

Substituting $\epsilon = -1$ into (36) yields an evolution equation for a collection of rigid disks. This evolution equation is identical to the area tensor evolution equation (28) except for the factor of two multiplying the fourth-order term in (36). This difference arises because the material interfaces composing the area tensor can stretch (26), whereas the disk-like particles cannot.

4. Closure Approximation

The evolution equation for the second-order area tensor contains the fourth-order area tensor, which is not calculated explicitly. In order to obtain a closed set of equations, a closure approximation is needed to approximate the fourth-order tensor in terms of the second-order tensor. An example of such an approximation is the quadratic closure (Doi and Ohta, 1991), which can be written in terms of the normalized tensors $\hat{\mathbf{A}}$ and $\hat{\mathcal{A}} \equiv \mathcal{A}/S_V$ as

$$\hat{\mathcal{A}}_{ijkl} = \hat{A}_{ij} \hat{A}_{kl}. \quad (37)$$

While (27) is exact for passive mixing, a closure approximation such as (37) can introduce errors into the solution. Similar closure problems arise in other microstructural tensor models, most notably in rigid-particle suspensions (Cintra and Tucker, 1995; Advani and Tucker, 1990; Hinch and Leal, 1976) and liquid crystals (Chaubal et al., 1995; Maffettone and Crescitelli, 1994; Bhawe et al., 1993). The methodology used here to create a closure approximation is

applicable to these other microstructural representations as well, although the actual closures will differ due to the differing physics governing the evolution of each microstructure. Therefore we will only briefly overview the closure approximation here, and reserve a more detailed treatment for a future publication (Wetzel and Tucker, 1998).

We begin by assuming that the fourth-order tensor will be approximated as a function of the second-order tensor only. Closures can depend on other quantities, such as the rate of deformation. However, such formulas lose their meaning when there is no flow, and so are not useful for predicting the influence of microstructure on final material properties. It will also be convenient to work in terms of the normalized tensors $\hat{\mathbf{A}}$ and $\hat{\mathcal{A}}$. From their definitions, these tensors satisfy the relationships

$$\hat{A}_{ii} = 1, \quad (38)$$

$$\hat{\mathcal{A}}_{ijkk} = \hat{A}_{ij}. \quad (39)$$

Note that $S_V = \text{tr}(\mathbf{A})$, so the full fourth-order tensor is easily recovered once $\hat{\mathcal{A}}$ has been approximated.

Cintra and Tucker (1995) showed that closure approximations based solely on the second-order tensor will be objective only if the microstructure is assumed to be orthotropic, i.e. to possess three orthogonal planes of symmetry. For orthotropic structures, the principal axes of $\hat{\mathbf{A}}$ must be the symmetry axes of the approximate $\hat{\mathcal{A}}$. Accordingly, formulating the closure approximation in the principal axis system of the second-order tensor greatly simplifies the closure procedure. Implementing the closure during numerical simulations requires rotation of these results back to the problem coordinates.

In the principal axis system, the fourth-order microstructural tensors of orthotropic structures have the form

$$\bar{\mathcal{A}}_{mm} = \begin{bmatrix} \bar{\mathcal{A}}_{11} & \bar{\mathcal{A}}_{12} & \bar{\mathcal{A}}_{13} & 0 & 0 & 0 \\ \bar{\mathcal{A}}_{21} & \bar{\mathcal{A}}_{22} & \bar{\mathcal{A}}_{23} & 0 & 0 & 0 \\ \bar{\mathcal{A}}_{31} & \bar{\mathcal{A}}_{32} & \bar{\mathcal{A}}_{33} & 0 & 0 & 0 \\ 0 & 0 & 0 & \bar{\mathcal{A}}_{44} & 0 & 0 \\ 0 & 0 & 0 & 0 & \bar{\mathcal{A}}_{55} & 0 \\ 0 & 0 & 0 & 0 & 0 & \bar{\mathcal{A}}_{66} \end{bmatrix} \quad (40)$$

where the tensor is presented in contracted notation (e.g., Jones, 1975). The symmetry of the fourth-order tensor reduces the number of independent components in (40) to six. A further reduction, to three independent components, is provided by the normalization relationships in (38, 39). A convenient choice for these three independent components is

$$\hat{\mathcal{A}}_{(1)} \equiv \bar{\mathcal{A}}_{11}, \quad \hat{\mathcal{A}}_{(2)} \equiv \bar{\mathcal{A}}_{22}, \quad \hat{\mathcal{A}}_{(3)} \equiv \bar{\mathcal{A}}_{33}, \quad (\hat{\mathcal{A}}_{(1)} \geq \hat{\mathcal{A}}_{(2)} \geq \hat{\mathcal{A}}_{(3)}). \quad (41)$$

These three scalar quantities must be functions of the eigenvalues of $\hat{\mathbf{A}}$, of which only two are independent due to (38). This reduces the general closure problem to the task of choosing three scalar functions, each depending on two eigenvalues of the second-order tensor

$$\hat{\mathcal{A}}_{(1)} = f_{(1)}(\hat{A}_{(1)}, \hat{A}_{(2)}), \quad \hat{\mathcal{A}}_{(2)} = f_{(2)}(\hat{A}_{(1)}, \hat{A}_{(2)}), \quad \hat{\mathcal{A}}_{(3)} = f_{(3)}(\hat{A}_{(1)}, \hat{A}_{(2)}). \quad (42)$$

To derive a specific closure for the area tensor we further assume that the distribution of differential areas matches that of a specific orthotropic structure, the general ellipsoid. The family of ellipsoids includes the limiting cases of spherical, cylindrical, and lamellar shapes frequently observed in mixtures. More importantly, in passive mixing a fluid domain that is ellipsoidal in one configuration will deform into an ellipsoid for any deformation that is homogeneous on the scale of the domain. Under these circumstances a closure based on ellipsoidal shapes will be exact for any structure generated by passive mixing. This argument also applies to any ellipsoidal distribution of area. For example, any complex structure which is initially isotropic, even though it does not consist of spherical particles, will maintain an ellipsoidal distribution of area for any deformation.

Equations (1, 2) show that the area tensor is a geometric quantity determined entirely by the shape of the interface within the averaging volume. For ellipsoids, a given second-order area tensor uniquely determines the shape of a corresponding ellipsoid, which in turn uniquely determines the fourth-order area tensor for that ellipsoid. Therefore, ellipsoids possess an exact closure *relationship* between the fourth-order and second-order area tensors. This relationship can be expressed implicitly in terms of the axis ratios of the ellipsoid (11), where the second-order components have already been given by (12–14) and the fourth-order components are (Appendix A)

$$\hat{\mathcal{A}}_{(i)} = \alpha_i \frac{\beta_{i1}E(\theta, k) + \beta_{i2}F(\theta, k) + \beta_{i3}\sqrt{1 - C^2}}{(1 - C^2)E(\theta, k) + C^2F(\theta, k) + CD\sqrt{1 - C^2}} \quad (43)$$

$i = 1$ to 3 (no sum on i). The coefficients α_i and β_{ij} are given in Table 2, and k and θ are defined by (15,16).

These exact relations cannot be rearranged to express the fourth-order tensor explicitly as a function of the second-order tensor. Since the computational cost of the closure needs to be low, we construct a convenient explicit function that closely approximates the exact closure relationship. This approximation is generated by choosing a functional form, constraining the form, and fitting the constrained function to data generated from the exact closure. The constraints force the closure to obey geometric symmetries, give exact results in the three limiting cases of Table 1, and have correct asymptotic behavior near those limits (Wetzel and Tucker, 1998).

Exact data for $\hat{\mathcal{A}}_{(1)}$, $\hat{\mathcal{A}}_{(2)}$, and $\hat{\mathcal{A}}_{(3)}$ as a function of $\hat{A}_{(1)}$ and $\hat{A}_{(2)}$ were generated using (12, 13, 43) for 127 fitting points encompassing the complete range of ellipsoidal shapes. The closure that we will use here is a third-order/second-order rational polynomial in terms of $\hat{A}_{(1)}$ and $\hat{A}_{(2)}$, having the form

Table 2
Coefficients for (43)

	$i = 1$	$i = 2$	$i = 3$
α_i	$\frac{1}{(1 - C^2)(1 - D^2)^2}$	$\frac{D^2}{(1 - D^2)^2(D^2 - C^2)^2}$	$\frac{C^2}{(1 - C^2)(D^2 - C^2)^2}$
β_{i1}	$(1 + C^2 + D^2 - 3C^2D^2)$	$D^2(1 - C^2)(-3C^2 + D^2 + D^4 + C^2D^2)$	$C^2(C^2 - 3D^2 + C^4 + C^2D^2)$
β_{i2}	$(-C^2 - 2D^2 + 3C^2D^2)$	$D^2(D^2 - C^2)(3C^2 - 2D^2 - C^2D^2)$	$C^4(D^2 - C^2)$
β_{i3}	$-CD(1 - D^2)$	$CD(1 - D^2)(2C^2 - D^4 - C^2D^2)$	$CD(2D^2 - C^4 - C^2D^2)$

$$\hat{A}_{(m)} = \frac{P(\hat{A}_{(1)}, \hat{A}_{(2)})}{Q(\hat{A}_{(1)}, \hat{A}_{(2)})}$$

$$\begin{aligned}
 P(\hat{A}_{(1)}, \hat{A}_{(2)}) = & c_{(m)1} + c_{(m)2}\hat{A}_{(1)} + c_{(m)3}\hat{A}_{(2)} + c_{(m)4}\hat{A}_{(1)}\hat{A}_{(2)} + c_{(m)5}\hat{A}_{(1)}^2 \\
 & + c_{(m)6}\hat{A}_{(2)}^2 + c_{(m)7}\hat{A}_{(1)}^2\hat{A}_{(2)} + c_{(m)8}\hat{A}_{(1)}\hat{A}_{(2)}^2 + c_{(m)9}\hat{A}_{(1)}^3 + c_{(m)10}\hat{A}_{(2)}^3, \\
 Q(\hat{A}_{(1)}, \hat{A}_{(2)}) = & 1 + c_{(m)11}\hat{A}_{(1)} + c_{(m)12}\hat{A}_{(2)} + c_{(m)13}\hat{A}_{(1)}\hat{A}_{(2)} + c_{(m)14}\hat{A}_{(1)}^2 + c_{(m)15}\hat{A}_{(2)}^2.
 \end{aligned}
 \tag{44}$$

The fitted coefficients $c_{(m)n}$ are given in Table 3. The procedure for calculating the remaining terms of (40) and rotating the tensor to the proper coordinate space is detailed elsewhere (Cintra and Tucker, 1995; Wetzel and Tucker, 1997). We will refer to this closure approximation as the RE, or rational ellipsoidal, closure. (The exact numerical values of the coefficients differ slightly from those reported by Wetzel and Tucker (1997) due to the use of different fitting data.)

Table 3
Closure coefficients $c_{(m)n}$ for the RE closure, (44). The horizontal line separates numerator and denominator coefficients

n	$m = 1$	$m = 2$	$m = 3$
1	0.1433751825	0.1433751825	0.9685744898
2	-0.6566650339	-0.5209453949	-2.5526857671
3	-0.5106016916	-0.6463213306	-2.5756669706
4	4.4349137241	2.3303190917	4.4520903005
5	3.5295952199	0.6031924921	2.2044050704
6	0.1229618909	5.1539592511	2.2485545147
7	-5.5556896198	-1.6481269200	-1.8811803355
8	-2.8284365891	-5.4494528976	-1.9023485762
9	-2.9144388828	-0.2256222796	-0.6202937932
10	0.2292109036	-3.7461520908	-0.6414620339
11	0.7257989503	0.6916858207	-1.2134964928
12	3.0941511876	3.1282643172	-1.2128608265
13	-4.7303686308	-4.7303686308	0.6004510415
14	-1.6239324646	-1.5898193351	0.2393747647
15	-3.1742364608	-3.2083495904	0.2162486576

As a measure of the quality of the fit, we use the rms error among six fitted components ($\hat{A}_{mm}, 1 \leq m \leq 6$, no sum on m) and all 127 data points. For the RE closure this error is 1.5×10^{-4} . (The components of \hat{A} are all order one.) In contrast, the quadratic closure of (37) has an rms error of 7.0×10^{-2} . Additionally, the quadratic closure does not match the exact fourth-order tensor values for spherical and cylindrical morphologies.

5. Microstructural evolution in flow fields

In this section we demonstrate the accuracy of the RE closure for modeling area tensor evolution. We also compare area tensor results with classical mixing principles, and demonstrate the interpretation of area tensors in terms of representative ellipsoids. Additionally, we illustrate the use of the area tensor as a field variable by modeling morphology development in steady flow between parallel plates.

5.1. Generation of reference data

Reference data for testing the accuracy of the tensor results was generated using a Lagrangian approach (Szeri and Leal, 1992, 1994). At a single material point the microstructure is represented by a large number of differential areas, each of which evolves during flow according to (25, 26). This scheme provides an exact rate of change for each area vector, without a closure approximation. The second- and fourth-order area tensors are reconstructed at any desired time by summing the contributions from each area vector. If area vector m has normal $\hat{\mathbf{n}}^m$ and magnitude dS^m , the reconstructed area tensors are

$$\begin{aligned} A_{ij} &= \frac{1}{V} \sum_m n_i^m n_j^m dS^m, \\ A_{ijkl} &= \frac{1}{V} \sum_m n_i^m n_j^m n_k^m n_l^m dS^m. \end{aligned} \tag{45}$$

We advance the vector evolution equations numerically using a fourth-order Runge–Kutta method with adaptive step-sizing. Numerical errors are minimized by working in double precision and placing low error tolerances on the stepping algorithm. Discretization errors are minimized by using approximately 100,000 area vectors over a hemisphere of orientation space. In the results that follow, the maximum deviation of any component of \hat{A} from the exact result is less than 10^{-5} , where the components of \hat{A} are all of order one.

Generating an array of differential areas to produce an initially isotropic area distribution is not straightforward. The spherical orientation space was discretized into a triangular mesh, with a normal vector defined through the centroid of each triangular mesh element. Each normal vector was then assigned an initial area dS^m proportional to the surface area of its associated spherical triangle (Wetzel and Tucker, 1997). The resulting array of area vectors produced fourth-order components \hat{A}_{ijkl} within 10^{-6} of the exact isotropic values.

While the Lagrangian approach gives highly accurate results without using a closure approximation, it is much more expensive computationally than the tensorial approach. For

example, generating reference data that was sufficiently accurate to determine the errors in the RE closure required storage and calculation of 300,000 scalars for each material point. The second-order area tensor summarizes this information using just 6 scalar components. This economy is multiplied many times over in a field problem, where one tracks the microstructure at many points within the flow field.

5.2. Accuracy of closures in homogeneous flows

We first test the area tensor and its closure approximations in homogeneous flows, where both the microstructure and the velocity gradient are independent of position. This reduces (27) to a set of ordinary differential equations for the area tensor components. Area tensor histories were generated by integrating (27) in time, using a fourth-order Runge–Kutta method with adaptive step-sizing. In all cases, the initial condition was an isotropic area tensor with unit trace.

These closure-based results were compared to the reference results described in the previous section. To evaluate the accuracy of the closure approximations we define an error tensor ϵ_{ij} as

$$\epsilon_{ij} = \frac{A_{ij}^{\text{ref}} - A_{ij}^{\text{closure}}}{\text{tr}(\mathbf{A})^{\text{ref}}}. \quad (46)$$

A convenient scalar measure of the error is

$$\epsilon = \sqrt{\frac{1}{2} \epsilon_{ij} \epsilon_{ji}} \quad (47)$$

and for transient flows we report the average of this quantity over time,

$$\epsilon^{\text{avg}} = \frac{1}{t_f} \int_0^{t_f} \epsilon(t) dt. \quad (48)$$

Table 4 summarizes the results of this study, showing the average error for the RE and quadratic closure approximations in various flows. We next examine in more detail the behavior of the biaxial stretching, simple shear, and combined stretching/shearing flow. The behavior in uniaxial elongation is similar to that in biaxial elongation, and will not be discussed further.

5.2.1. Biaxial elongation

For biaxial stretching along the x_2 and x_3 axes, the velocity gradient tensor is

$$L_{ij} = \frac{\partial v_i}{\partial x_j} = \begin{bmatrix} -2B & 0 & 0 \\ 0 & B & 0 \\ 0 & 0 & B \end{bmatrix}. \quad (49)$$

Due to symmetry, $A_{22} = A_{33}$ and all off-diagonal tensor components equal zero in this problem. Fig. 4(a) and (b) show the initial evolution of the A_{11} and A_{22} components in this flow. Most of the area rotates to lie in the 2–3 plane, where it stretches rapidly. A_{11} soon

Table 4
Average errors of RE and quadratic closures in homogeneous flows

Flow	Final strain	ϵ^{avg} , RE	ϵ^{avg} , Quadratic
Uniaxial elongation	$Ut = 1.4$	2.6×10^{-5}	2.1×10^{-2}
Biaxial elongation	$Bt = 1.4$	1.5×10^{-4}	9.5×10^{-2}
Simple shear	$Gt = 7.0$	1.4×10^{-4}	9.5×10^{-2}
Three-stage flow (see (55))	$Gt = 30$	1.7×10^{-3}	1.1×10^{-1}

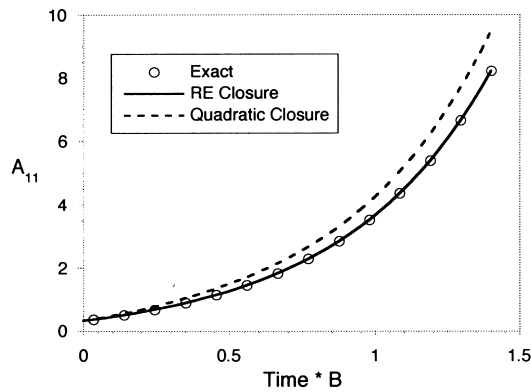
becomes the largest component of \mathbf{A} , and continues to grow rapidly with time. Conversely, A_{22} decays rapidly and, after a short time, very little area is normal to the x_2 axis. The RE and quadratic closures both exhibit correct qualitative behavior in this flow, though the quantitative accuracy of the RE closure is much better, as shown in Table 4.

The area tensor at $Bt = 1.4$ is

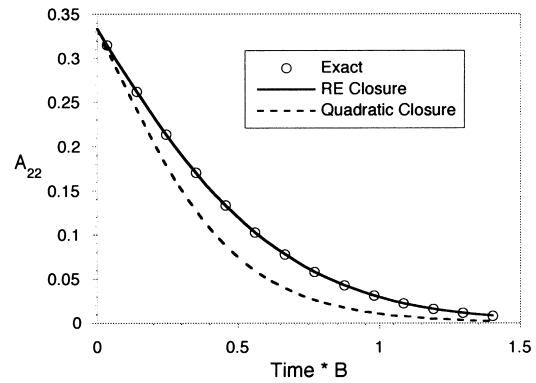
$$\mathbf{A} = \begin{bmatrix} 8.22 & 0 & 0 \\ 0 & 0.00812 & 0 \\ 0 & 0 & 0.00812 \end{bmatrix}. \quad (50)$$

If the initial area tensor represented a sphere of unit radius, then using (17) and assuming constant volume, this area tensor represents an oblate spheroid of minor semi-axis $r_1 = 0.063$ and major semi-axes $r_2 = r_3 = 4.0$.

Fig. 5 shows the trace of \mathbf{A} in biaxial elongational flow. After an initial transient, the trace of \mathbf{A} , which measures the specific area of the mixture, grows exponentially with time. This behavior is consistent with the well-known mixing principle that elongational flows produce exponential growth in surface area (Erwin, 1978). Using the observation that in biaxial stretching the area tensor becomes uniaxial at large strains, (29) simplifies to $\dot{S}_V = 2S_V B$ or



(a) A_{11} component



(b) A_{22} component

Fig. 4. Evolution of initially isotropic area tensor in biaxial elongation. Note the different vertical scales on the plots.

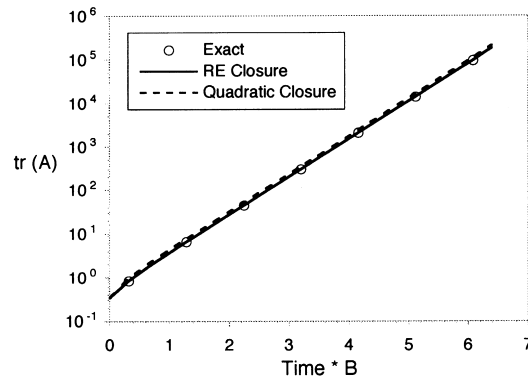


Fig. 5. Exponential growth of $\text{tr}(\mathbf{A})$ during large-strain biaxial elongation.

$$S_V/S_V^0 = \exp(2Bt) \quad (51)$$

which agrees with the limiting behavior of Fig. 5.

Both the RE and quadratic closures exhibit correct asymptotic behavior for large biaxial strains. However, the quantitative accuracy of the two closures is quite different. For large strains, the relative error in the trace, defined as $[\text{tr}(\mathbf{A})^{\text{closure}} - \text{tr}(\mathbf{A})^{\text{ref}}]/\text{tr}(\mathbf{A})^{\text{ref}}$, reaches a steady value of 1.6×10^{-1} for the quadratic closure and 1.0×10^{-4} for the RE closure. (The logarithmic scale of Fig. 5 obscures these differences in accuracy.)

5.2.2. Simple shear

Fig. 6(a)–(d) show the evolution of the area tensor during a simple shear flow, in which the velocity gradient is

$$L_{ij} = \begin{bmatrix} 0 & G & 0 \\ 0 & 0 & 0 \\ 0 & 0 & 0 \end{bmatrix}. \quad (52)$$

By symmetry, $A_{23} = A_{31} = 0$ in this flow.

In this flow, most of the area rotates to have a normal vector close to the x_2 axis, so A_{22} becomes the largest component of the area tensor. Again, assuming that the initial area tensor corresponds to a sphere of unit radius, the area tensor at $Gt = 7.0$,

$$\mathbf{A} = \begin{bmatrix} 0.0717 & -0.480 & 0 \\ -0.480 & 3.44 & 0 \\ 0 & 0 & 0.165 \end{bmatrix} \quad (53)$$

corresponds to an ellipsoid with principal semi-axes of length $r_3 = 7.6$, $r_2 = 0.90$, and $r_1 = 0.15$. The r_3 axis lies in the x_1 – x_2 plane and is oriented 8.0° above the x_1 axis.

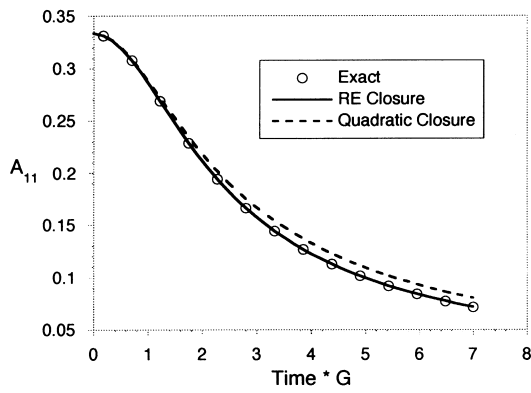
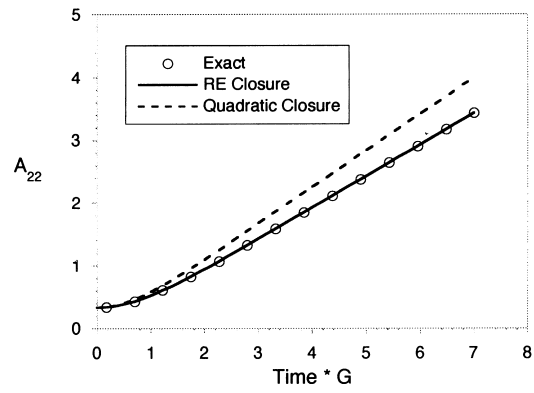
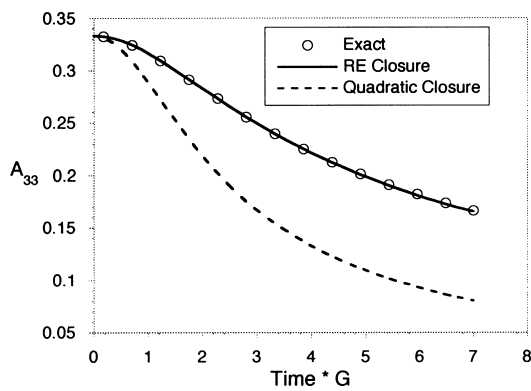
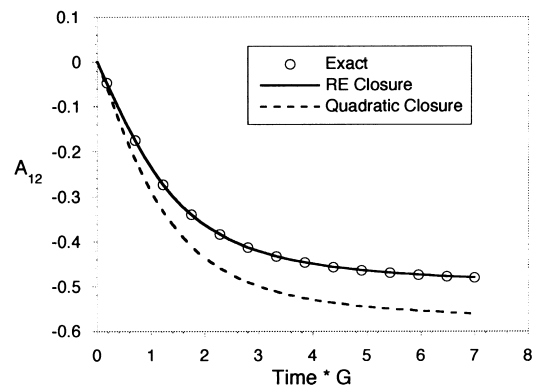
(a) A_{11} component(b) A_{22} component(c) A_{33} component(d) A_{12} component

Fig. 6. Evolution of initially isotropic area tensor in simple shear. Note the different vertical scales on the plots.

Fig. 6(a)–(d) and Table 4 show that the RE closure is much more accurate than the quadratic closure in simple shear. Both closures exhibit linear growth of $\text{tr}(\mathbf{A})$ at large strains, consistent with the classical mixing principle that shearing flows produce linear growth in interfacial areas (Mohr et al., 1957). (The plot of $\text{tr}(\mathbf{A})$ vs time is essentially identical to Fig. 6(b), since A_{22} dominates the trace at large times.) However, the quadratic closure gives an incorrect rate of growth. This is a serious limitation of the quadratic closure, since many mixing devices use very large shear strains. The exact rate of area growth can be calculated using (29), which for simple shear, simplifies to $\dot{S}_V = -GA_{12}$. Using the finite deformation equation (32), it can be shown (Wetzel, 1997) that at large strains A_{12}/S_V^0 approaches a value of $-1/2$ for an initially spherical domain. This result leads to the linear area growth law

$$S_V/S_V^0 = 1 + (Gt)/(2S_V^0). \quad (54)$$

5.2.3. Three-stage flow

A more demanding test is provided by a three-stage flow, where

$$\begin{aligned}
 L_{ij} &= \begin{bmatrix} 0 & G & 0 \\ 0 & 0 & 0 \\ 0 & 0 & 0 \end{bmatrix} \quad \text{for } 0 < Gt \leq 10, \\
 L_{ij} &= \begin{bmatrix} -U & 0 & 0 \\ 0 & -U & 0 \\ 0 & G & 2U \end{bmatrix} \quad \text{for } 10 < Gt \leq 20, \\
 L_{ij} &= \begin{bmatrix} 2U & 0 & 0 \\ 0 & -U & 0 \\ 0 & G & -U \end{bmatrix} \quad \text{for } 20 < Gt \leq 30
 \end{aligned} \tag{55}$$

and $G = 20 U$. The first stage is simple shear, the second stage combines simple shear with uniaxial elongation, and the third stage is identical to the second except that the direction of elongation has been changed. Fig. 7(a)–(f) show the A_{11} , A_{22} , A_{33} , A_{23} , A_{13} , and A_{12} components for the flow. The accuracy of the RE closure is excellent over all six tensor components and during the entire flow history, while the quadratic closure develops some significant errors.

5.3. Application to a field problem

To illustrate the applicability of the area tensor to field problems, we consider steady pressure-driven flow between parallel plates as shown in Fig. 8. For a gap height of $2H$ and centerline velocity v_c , the Newtonian velocity profile is

$$v_1(x_2) = v_c[1 - (x_2/H)^2] \tag{56}$$

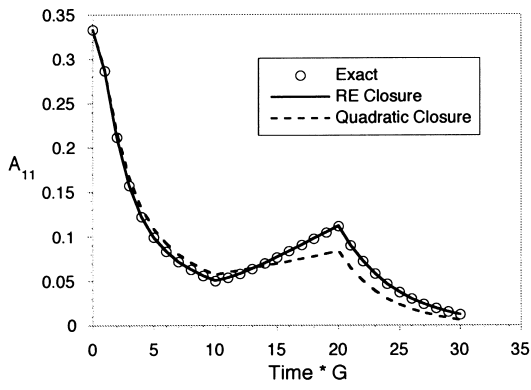
with x_1 the flow direction and x_2 the gapwise direction. Material points move along streamlines of constant x_2 , and a material point at any position x_1 has a residence time of $t = x_1/v_1$. The shear rate,

$$G = -\frac{\partial v_1}{\partial x_2} = v_c \frac{2x_2}{H^2} \tag{57}$$

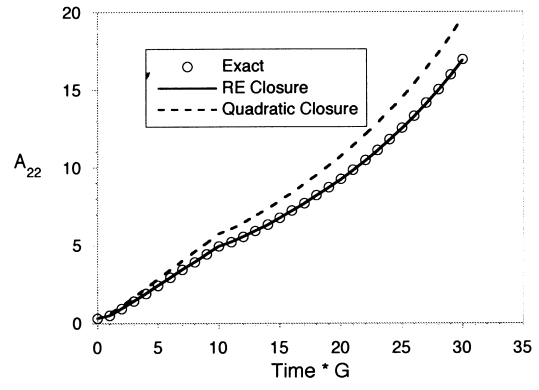
is independent of x_1 , so at steady state any point (x_1, x_2) in the flow field has accumulated a shear strain γ equal to

$$\gamma = Gt = \frac{2x_1x_2}{(H^2 - x_2^2)} \tag{58}$$

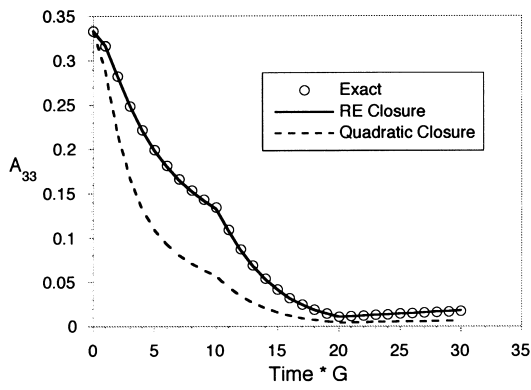
since entering the flow. In Section 5.2.2 we calculated area tensor evolutions in simple shear flow as a function of strain [Fig. 6(a)–(b)]. Using (58), we can map these results from a



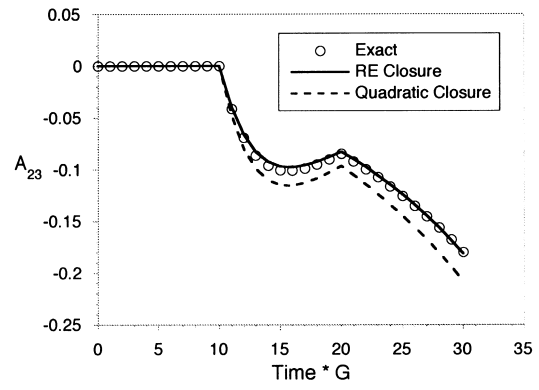
(a) A_{11} component



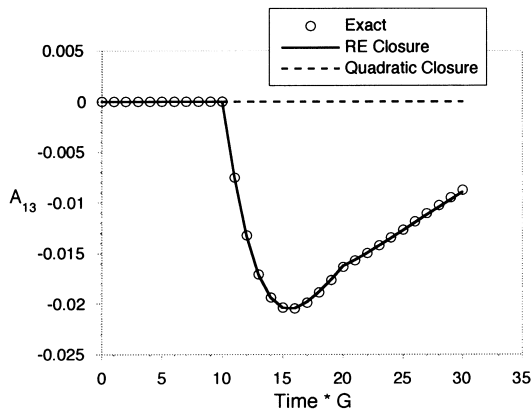
(b) A_{22} component



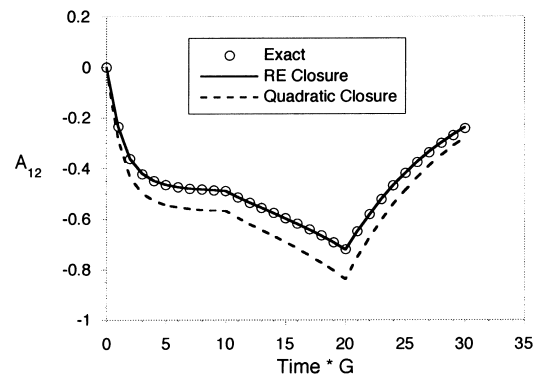
(c) A_{33} component



(d) A_{23} component



(e) A_{13} component



(f) A_{12} component

Fig. 7. Evolution of initially isotropic area tensor during three-stage elongational/shear flow.

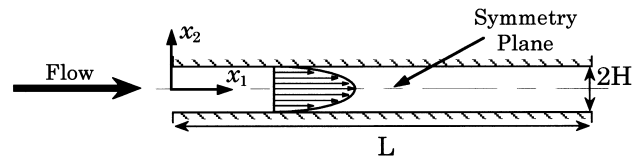


Fig. 8. Geometry for strip flow. The upper half of the domain is plotted in Fig. 9(a) and (b).

function of strain to a function of position in the strip flow geometry. The resulting area tensor field represents the steady-state microstructure for the flow.

The velocity at the wall is zero, so the residence time and accumulated strain there are infinite. In practice, either diffusion or dispersion will become important in a thin boundary layer near the wall, or else the process will not reach steady state in this zone. We ignore this detail, and only plot data up to $x_2 = 0.95 H$.

Fig. 9(a) and (b) show results for the upper half of a channel of aspect ratio $L/H = 20$ and an isotropic inlet condition with $S_V = 1$. The contours indicate the logarithm of the trace of the tensor, a measure of morphological length scale. Larger values of S_V indicate a finer microstructure. The vectors indicate the orientation and anisotropy of the morphology, with longer vectors representing highly aligned morphologies and dots representing morphologies which are isotropic in the x_1 - x_2 plane. At the midplane the shear rate is zero and the inlet microstructure is transported with no deformation. The trace of the area tensor increases

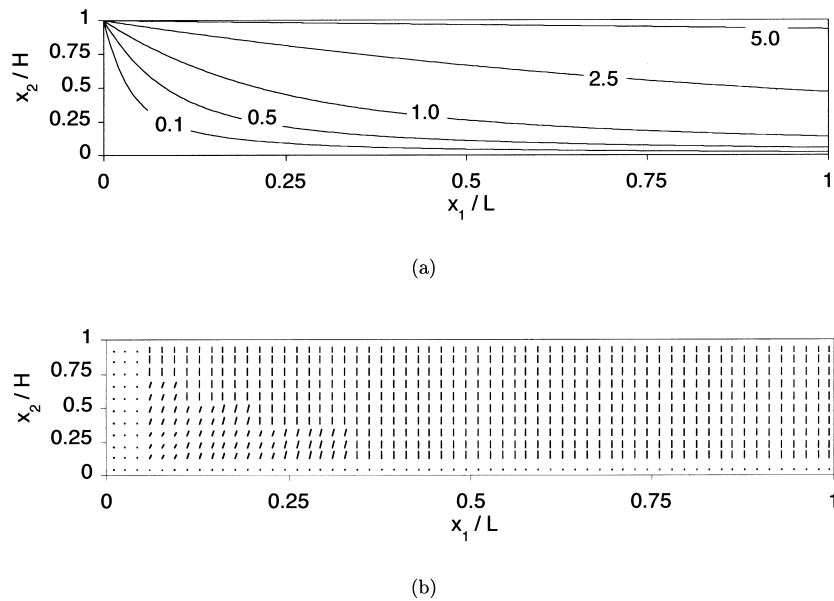


Fig. 9. Steady state area tensor distribution for strip flow. Region plotted is upper half of domain shown in Fig. 8: (a) contours of $\log S_V$; (b) principal direction and anisotropy of \mathbf{A} . Vectors point in direction of largest eigenvalue of \mathbf{A} . The vector length is proportional to the difference in magnitude between the two eigenvalues in the x_1 - x_2 plane. A unit length vector indicates a uniaxial tensor, while a dot (a vector of zero length) indicates an in-plane isotropic tensor.

toward the channel walls, because of higher shear rates and longer residence times, and also increases in the flow direction, due to increasing magnitude of accumulated shear. The tensor also becomes highly oriented and dominated by the A_{22} term toward the edges and the outlet of the channel.

The area tensor at $x_2 = 0.95 H$ at the exit is nearly uniaxial with a trace equal to 195.1, so we can treat this as a lamellar structure. Using (8) and Table 1 with a dispersed-phase volume fraction $\phi = 0.10$, this tensor represents a lamellar morphology with an average sheet thickness of 1.0×10^{-3} . At the exit midplane, the triaxial tensor with $S_V = 1$ corresponds to a spherical geometry with a characteristic radius of 0.30. These results agree qualitatively with the “skin-core” effect observed experimentally in injection-molded polymer blends (Fellahi et al., 1996), and demonstrate the highly localized morphology that can develop during even simple non-homogeneous flows.

6. Conclusions

Mixtures whose microstructure is too small to resolve exactly in a numerical simulation can be modeled using average measures of the local morphology. For this purpose we have defined the area tensor, which provides information on the size, shape, and orientation of the microstructure. This information is necessary both for accurate simulation of mixing and for prediction of many mixture properties. In mixtures containing geometrically complex interfaces, the area tensor is directly (and exactly) related to the rate of area growth in passive mixing, and to the interfacial tension contribution to the extra stress. Therefore, the area tensor is both a convenient expression of mixture structure, as well as a fundamentally significant quantity that governs mixing dynamics and rheological behavior.

We have derived an evolution equation for the second-order area tensor that is exact for passive mixing. This rate equation contains the fourth-order area tensor, which can be approximated in terms of the second-order area tensor. We have formulated such a closure approximation, by assuming that any morphology can be represented by a prototype ellipsoid. An exact implicit closure relationship has been derived for ellipsoidal microstructures, and approximated with an explicit rational polynomial function. This explicit closure approximation (the RE closure) is very accurate, and allows one to use the second-order area tensor as a microstructural state variable in mixing flows without introducing significant errors.

The area tensor model successfully captures the classical mixing behaviors of exponential interfacial area growth in elongational flows and linear growth in simple shear flow. However, the area tensor model supplements this magnitude information with information on the shape and orientation of the interfaces. The differential form of the area tensor evolution equation allows modeling the area tensor in any flow whose velocity field can be resolved locally as a function of time. This capability has been demonstrated by solving for the steady morphological field for initially spherical domains subjected to flow between parallel plates. The calculation predicted morphological gradients, due to the differences in shear rate and residence time experienced by different material points. These results agree qualitatively with experimental results, and demonstrate the value of the local morphological descriptions provided by the area tensor method.

The purpose of this study is to present a general framework by which a variety of processes and physics can eventually be modeled. The area tensor results presented here model mixtures with passive interfaces, which is the simplest implementation of this framework. However, the evolution equation has been presented in a general form which allows incorporation of additional process physics. Phenomena that might be added to this framework include surface tension–driven relaxation, surface tension–driven breakup, and coalescence, as well as the influence of unequal component viscosities. Many other opportunities exist for the advancement of this approach, including application of the area tensor approach to complex flows and geometries using numerical methods, direct coupling between the morphology and rheology in a flow simulation, and the development of relations between the area tensor and physical properties such as rheology, permeability, and stiffness.

Appendix A Derivation of exact area tensor relations

For the general ellipsoid defined by (10) the components of the unit vector $\hat{\mathbf{n}}$ normal to the surface are

$$\hat{n}_1 = \frac{\cos \theta}{\sqrt{C^2 \sin^2 \theta \cos^2 \phi + D^2 \sin^2 \theta \sin^2 \phi + \cos^2 \theta}}, \quad (\text{A.1})$$

$$\hat{n}_2 = \frac{D \sin \theta \sin \phi}{\sqrt{C^2 \sin^2 \theta \cos^2 \phi + D^2 \sin^2 \theta \sin^2 \phi + \cos^2 \theta}}, \quad (\text{A.2})$$

$$\hat{n}_3 = \frac{C \sin \theta \cos \phi}{\sqrt{C^2 \sin^2 \theta \cos^2 \phi + D^2 \sin^2 \theta \sin^2 \phi + \cos^2 \theta}} \quad (\text{A.3})$$

and the incremental area dS is

$$dS = r_1^2 \frac{1}{CD} \sin \theta \sqrt{C^2 \sin^2 \theta \cos^2 \phi + D^2 \sin^2 \theta \sin^2 \phi + \cos^2 \theta} d\theta d\phi \quad (\text{A.4})$$

where

$$z_1 = r_1 \cos \theta, \quad z_2 = r_2 \sin \theta \sin \phi, \quad z_3 = r_3 \sin \theta \cos \phi \quad (\text{A.5})$$

and the axis ratios C and D are defined in (11). Substituting these relations into the definition of the second-order area tensor, (1), yields

$$A_{22} = \frac{1}{V} \int_0^{2\pi} \int_0^\pi \frac{r_1^2 (D/C) \sin^3 \theta \sin^2 \phi}{\sqrt{C^2 \sin^2 \theta \cos^2 \phi + D^2 \sin^2 \theta \sin^2 \phi + \cos^2 \theta}} d\theta d\phi \quad (\text{A.6})$$

$$A_{33} = \frac{1}{V} \int_0^{2\pi} \int_0^\pi \frac{r_1^2 (C/D) \sin^3 \theta \cos^2 \phi}{\sqrt{C^2 \sin^2 \theta \cos^2 \phi + D^2 \sin^2 \theta \sin^2 \phi + \cos^2 \theta}} d\theta d\phi. \quad (\text{A.7})$$

The integrals can be performed using the transformations of Maas (1992). The normalized area tensors \hat{A}_{22} and \hat{A}_{33} are found by dividing (A6, A7) by the surface area of an ellipsoid, given by Legendre (1811) as

$$S_{\text{ellipsoid}} = \frac{2\pi r_1^2}{DC} \frac{1}{\sqrt{1-C^2}} ((1-C^2)E(\theta, k) + C^2F(\theta, k) + CD\sqrt{1-C^2}) \quad (\text{A.8})$$

to yield (13, 14), where the arguments k and θ are defined in (15, 16). Equation (12) results from the normalization condition, (38).

Similarly, substituting (A.1–A.4) into the definition of the fourth-order area tensor, (2), yields

$$A_{1111} = \frac{1}{V} \int_0^{2\pi} \int_0^\pi \frac{r_1^2(1/CD) \sin \theta \cos^4 \theta}{(C^2 \sin^2 \theta \cos^2 \phi + D^2 \sin^2 \theta \sin^2 \phi + \cos^2 \theta)^{3/2}} d\theta d\phi, \quad (\text{A.9})$$

$$A_{2222} = \frac{1}{V} \int_0^{2\pi} \int_0^\pi \frac{r_1^2(D^3/C) \sin^5 \theta \sin^4 \phi}{(C^2 \sin^2 \theta \cos^2 \phi + D^2 \sin^2 \theta \sin^2 \phi + \cos^2 \theta)^{3/2}} d\theta d\phi, \quad (\text{A.10})$$

$$A_{3333} = \frac{1}{V} \int_0^{2\pi} \int_0^\pi \frac{r_1^2(C^3/D) \sin^5 \theta \cos^4 \phi}{(C^2 \sin^2 \theta \cos^2 \phi + D^2 \sin^2 \theta \sin^2 \phi + \cos^2 \theta)^{3/2}} d\theta d\phi. \quad (\text{A.11})$$

Solving these integrals using the transformations of Maas (1994) and normalizing by (A.8) yields the exact fourth-order area tensor relations of (43).

More detailed derivations of all of these relations are given in Wetzel and Tucker (1997).

References

- Advani, S.G., Tucker, C.L., 1990. Closure approximations for three-dimensional structure tensors. *J. Rheol.* 34, 367–386.
- Batchelor, G.K., 1970. The stress system in a suspension of force-free particles. *J. Fluid Mech.* 41, 545–570.
- Bhave, A.V., Menon, R.K., Armstrong, R.C., Brown, R.A., 1993. A constitutive equation for liquid–crystalline polymer solutions. *J. Rheol.* 37, 413–441.
- Chaubal, C.V., Leal, L.G., Fredrickson, G.H., 1995. A comparison of closure approximations for the Doi theory of LCPs. *J. Rheol.* 39, 73–103.
- Chella, R., Ottino, J.M., 1985. Stretching in some classes of fluid motions and asymptotic mixing efficiencies as a measure of flow classification. *Arch. Rat. Mech. Anal.* 90, 15–42.
- Cintra, J.S., Jr, Tucker, C.L., 1995. Orthotropic closure approximations for flow-induced fiber orientation. *J. Rheol.* 39, 1095–1122.
- Doi, M., 1987. Microscopic basis for the viscoelasticity of suspensions. In Safran S.S., Clark M. (eds.), *Physics of Complex and Supermolecular Fluids*, Wiley, New York. 661–630.
- Doi, M., Ohta, T., 1991. Dynamics and rheology of complex interfaces I. *J. Chem. Phys.* 95, 1242–1248.
- Erwin, L., 1978. Theory of laminar mixing. *Polym. Eng. Sci.* 18, 1044–1048.
- Fellahi, S., Davis, B.D., Fisa, B., 1996. Morphological stability in injection-moulded high-density polyethylene/polyamide-6 blends. *Polymer* 37, 2615–2626.
- Gradshteyn, I.S., Ryzhik, I.M., 1994. *Table of Integrals, Series, and Products*. 5th. Academic Press, New York.
- Guenther, G.K., Baird, D.G., 1996. An evaluation of the Doi–Ohta theory for an immiscible polymer blend. *J. Rheol.* 40, 1–20.
- Hinch, E.J., Leal, L.G., 1976. Constitutive equations in suspension mechanics. Part 2. Approximate forms for a suspension of rigid particles affected by Brownian rotations. *J. Fluid Mech.* 76, 187–208.

- Jones, R.M., 1975. *Mechanics of Composite Materials*. McGraw-Hill, New York.
- Lee, H.M., Park, O.O., 1994. Rheology and dynamics of immiscible polymer blends. *J. Rheol.* 38, 1405–1425.
- Legendre, A.M., 1811. *Exercices de Calcul Integral*, Vol. I. Huzard–Courcier, Paris.
- Lehmer, D.H., 1950. Approximations to the area of an n -dimensional ellipsoid. *Can. J. Math.* 2, 267–282.
- Maas, L.R.M., 1994. On the surface area of an ellipsoid and related integrals of elliptic integrals. *J. Comp. Appl. Math.* 51, 237–249.
- Maffettone, P.L., Crescitelli, S., 1994. The rigid rod model for nematic polymers: testing closure approximations with bifurcation analysis. *J. Rheol.* 38, 1559–1570.
- Mohr, W.D., Saxton, R.L., Jepson, C.H., 1957. Mixing in laminar-flow systems. *Ind. Eng. Chem.* 49, 1855–1856.
- Ottino, J.M., Ranz, W.E., Macosko, C.W., 1981. A framework for description of mechanical mixing of fluids. *AIChE J.* 27, 565–577.
- Rosenkilde, C.E., 1967. Surface-energy tensors. *J. Math. Phys.* 8, 84–97.
- Spencer, R.S., Wiley, R.M., 1951. The mixing of very viscous liquids. *J. Colloid Sci.* 6, 133–145.
- Szeri, A.J., Leal, L.G., 1992. A new computational method for the solution of flow problems of microstructured fluids. Part 1. Theory. *J. Fluid Mech.* 242, 549–576.
- Szeri, A.J., Leal, L.G., 1994. A new computational method for the solution of flow problems of microstructured fluids. Part 2. Inhomogeneous shear flow of a suspension. *J. Fluid Mech.* 262, 171–204.
- Takahashi, Y., Kurashima, N., Noda, I., 1994. Experimental tests of the scaling relation for textured materials in mixtures of two immiscible fluids. *J. Rheol.* 38, 699–712.
- Vinckier, I., Moldenaers, P., Mewis, J., 1996. Relationship between rheology and morphology of model blends in steady shear flow. *J. Rheol.* 40, 613–631.
- Wetzel, E.D. 1997. Unpublished research results.
- Wetzel, E.D., Tucker, C.L., 1997. Area tensors for modeling morphology during laminar liquid-liquid mixing. Technical report UIUL-ENG 97-4014. University of Illinois.
- Wetzel, E.D., Tucker, C.L., 1998. Closure approximations for microstructured fluids. Manuscript in preparation.